Global transport of passive tracers in conventional and superparameterized climate models: Evaluation of multi-scale methods

D. Rosa,[1] J. F. Lamarque,[2] and W. D. Collins[1]

Received 24 September 2012; accepted 25 September 2012; published 30 October 2012.

[1] The global transport of the surface-emitted short-lived passive tracers radon and methyl iodide is simulated in a cloud-resolving Global Climate Model (GCM) for the first time and compared against simulations with a conventional GCM in which cloud processes are not resolved. Both models are operated in chemical transport mode in which the large scale flow is set to observationally derived dynamic and thermodynamic fields from a meteorological reanalysis. Simulated vertical profiles of tracers concentrations from both models are compared with profiles observed in situ. The comparisons suggest that the cloud-resolving GCM is, to a small degree, better than the conventional GCM in reproducing the vertical gradients and hence the convective entrainment and detrainment of passive tracers. Contrasting only simulated climatological maps of tracers concentrations from the two models, we find consistent and appreciable relative differences that create a quadrupole pattern in the vertical direction. Relative to the conventional GCM, the tracer concentrations from the cloud-resolving GCM results are depleted from the surface to 1 km and from 4 to 12 Km and enriched from 1 to 4 km and above 12 km. This might have important implications for climate and atmospheric chemistry simulations but require further investigations.

Citation: Rosa, D., J. F. Lamarque, and W. D. Collins (2012), Global transport of passive tracers in conventional and superparameterized climate models: Evaluation of multi-scale methods, *J. Adv. Model. Earth Syst., 4,* M10003, doi:10.1029/2012MS000206.

1. Introduction

[2] Accurate simulations for the transport of radiatively active atmospheric compounds are essential for the fidelity of climate projections. Reliable atmospheric transport models are also needed to determine local pollution burdens from known remote sources and to estimate the distribution of remote sources from local burdens.

[3] Atmospheric transport from cloud convection is particularly important for the vertical distribution of short-lived atmospheric compounds such as ozone and aerosols [*Mahowald et al.*, 1995; *Tang et al.*, 2011]. The radiative forcing by ozone is a significant driver for climate change [*Ramaswamy et al.*, 2001], and it is also an important pollutant in the set of compounds that govern surface air quality [*World Health Organization*, 2006]. The concentrations of tropospheric ozone and its precursors are strongly influenced by convective activity [*Lelieveld and Crutzen*, 1994; *Stevenson et al.*, 2006]. Likewise, aerosols can cause large direct and indirect radiative forcings that are significant drivers of climate change, but are subject to large uncertainties due to incomplete understanding of the interactions between aerosols and other components of the climate system like clouds and surface albedo [*Forster et al.*, 2007]. The effects of vertical dispersal are one of the principal sources of uncertainty in these estimates of radiative forcing [*Schulz et al.*, 2006].

[4] Generally, while large-scale flow operates from synoptic to global spatial and temporal scales, cloud convection transports atmospheric compounds from the planetary boundary layer (PBL) to the upper troposphere across vertical and horizontal spatial scales of kilometers and on time scales from hours to a day. Therefore, the horizontal and vertical distributions of passive tracers with characteristic lifetimes close to the timescales of convective activity can be highly heterogeneous in space and time and can retain a strong dependence on the distribution of sources and sinks.

[5] The main purpose of this study is to compare global simulations of short-lived surface-emitted passive tracers performed with parameterized and cloud-resolving

[1]Department of Earth and Planetary Science, University of California, Berkeley, California, USA.
[2]National Center for Atmospheric Research, Boulder, Colorado, USA.

1942-2466/12/2012MS000206

treatments of cloud convective transport. We evaluate the fidelity of the simulations by comparing the simulated against observed vertical concentration profiles. We conducted two simulations using the National Center for Atmospheric Research Global Climate Model (GCM) Community Atmosphere Model version 3 (CAM) [*Collins et al.*, 2006] with identical meteorological analyses but with two alternative treatments of cloud convection within each atmospheric column.

[6] The first treatment of cloud convection is based upon an ersatz about the statistical behavior of individual convecting clouds that determines the net vertical transport of a mesoscale ensemble of convecting cloud systems [*Hack*, 1994; *Zhang and Mcfarlane*, 1995; *Boville and Bretherton*, 2003]. It serves as the default treatment of cloud convection in CAM. In addition to the treatment we test here, there are several parametric formulations for treating cloud convection that are commonly used for chemical transport and climate simulations. The diversity among these representations of cloud convection is the most likely cause for much of the spread in chemical distributions [*Hoyle et al.*, 2011; *Zhang et al.*, 2008; *Tost et al.*, 2010].

[7] Hence, we investigate a second treatment of cloud convection using the "Super-Parameterized" CAM (SPCAM) in which the convective transport is determined from a cloud-resolving model (CRM) embedded in CAM that explicitly simulates physical and dynamical processes at the cloud scale [*Khairoutdinov et al.*, 2005]. This treatment can in principle replace, or in practice serve as a benchmark for current cloud parameterizations since its computational cost is about two orders of magnitude higher than that of CAM.

[8] SPCAM is a promising alternative to the current approaches for climate predictions. Atmospheric general circulation simulations using SPCAM and CAM have comparable biases in precipitation, precipitable water, top-of-the atmosphere radiative fluxes, and cloud radiative forcing with respect to observed climatologies [*Khairoutdinov et al.*, 2005, 2008]. However, SPCAM exhibits more realistic diurnal variability of non-drizzle precipitation and convective intraseasonal variability than CAM. CRMs, including the one embedded in SPCAM, produce more realistic simulations of atmospheric columns forced with a variety of observed meteorological regimes compared to models utilizing conventional convective parameterizations [*Xie et al.*, 2002; *Xu et al.*, 2002].

[9] Our numerical experiments are specifically designed to understand the implications for climate and pollutant dispersion simulations by comparing SPCAM to CAM in a controlled large-scale flow. We operate both models in the Chemical Transport Model (CTM) mode in which we set the large-scale flow to observationally derived dynamic and thermodynamic fields derived from meteorological reanalysis. Therefore the lateral winds governing the transport from the large scale atmospheric flows are identical and reasonably realistic in both simulations. Feedbacks from, and hence divergent simulations due to, differences in cloud-scale convective processes are not permitted. Due to this experimental design, contrasting passive tracer distributions should arise primarily from differences in the sub-grid vertical convective transport.

[10] It is well known that simulated concentrations of tracer compounds are sensitive to the treatment of convective processes. Differences in concentrations between simulations and observations and among simulations range from a few percent to much greater values, and in general the discrepancies are inversely proportional to the tracer lifetimes [*Mahowald et al.*, 1995; *Jacob et al.*, 1997; *Folkins et al.*, 2006; *Donner et al.*, 2007; *Tost et al.*, 2010]. We apply the CTM framework to radon-222 (Rn) and methyl iodide (CH_3I) following previous studies [*Donner et al.*, 2007, and references therein]. These tracers have short lifetimes that make their concentrations more sensitive to transport processes, do not evolve through complex chains of chemical reactions and do not interact strongly with the hydrological cycle. Nonetheless, our results can inform subsequent investigations about radiatively active compounds and pollutants that have lifetimes comparable to the lifetimes of the tracers used in this study but require greater modeling complexity.

[11] To quantify the fidelity of the models to *in situ* tracer measurements, we propose a metric for the vertical profile of tracer concentrations designed to highlight differences in the effects of convective entrainment and detrainment between the two simulations.

[12] Instead of using short-lived passive tracer concentrations to investigate vertical transport from cloud convection, one could compare the vertical velocities of convective air masses and have a more direct test for the velocity spectrum produced by convective parameterizations. Observations of these velocity fields are becoming more readily available thanks to the increasingly widespread deployment of Doppler radar instruments [*May and Rajopadhyaya*, 1999; *Uma and Rao*, 2009], but useful data still remain relatively scarce due to the inherent difficulties of collecting these observations from aircraft in dangerous environmental conditions [*Lemone and Zipser*, 1980; *Lucas et al.*, 1994].

2. Methods

[13] We simulate the global transport of two passive tracers using CAM and SPCAM in CTM mode over the period 1996-2006. In these experiments, the tracers are emitted at the surface of the Earth, and the models are forced by meteorological reanalysis. Test and control simulations from SPCAM and CAM respectively are obtained by using the super-parameterized and conventional treatments of cloud convection. The volume mixing ratio (VMR) vertical profiles and Local Convective Indices (LCI) of the tracers from CAM and SPCAM are compared against observational estimates from field campaigns. The LCI measures the concentration of the tracer relative change with height to quantify the fractional changes in VMR due to entrainment and/or detrainment between convection and its surrounding environment (see section 2.5 for more details). Since the LCI is based upon relative changes in the vertical direction, it is insensitive to local errors in the absolute

magnitude of modeled versus actual emissions. Outside of convective systems, the LCI measures large-scale cross-isentropic gradients in tracer concentration imposed by sources and vertical mixing upwind of the region of interest and by large-scale vertical motions resolved by the model. When possible the comparisons are *precise*, that is the simulated and observed period match exactly. Otherwise, the comparisons are *climatological*, that is the long-term simulated and observed intra-annual period match.

2.1. Global Circulation Model

[14] We use the CAM version 3.5.36 from National Center for Atmospheric Research with a latitudinal and longitudinal horizontal resolution of $1.9^\circ \times 2.5^\circ$, a vertical discretization of twenty-eight levels, the finite-volume dynamical core, and a time step of thirty minutes. We run CAM in CTM mode [*Mahowald et al.*, 1997; *Lamarque et al.*, 2011] using six-hourly meteorological reanalysis data from the National Center for Environmental Prediction [*Kalnay et al.*, 1996]. Vertical profiles of horizontal winds and temperature, and surface values of pressure, wind stress, sensible heat flux, and water vapor flux are linearly interpolated in time and space onto the atmospheric grid of CAM. The modeled atmospheric fields are output every three simulated hours.

2.2. Planetary Boundary Layer and Cloud Convection Treatments

[15] In CAM, PBL and cloud convective processes are not resolved because its grid is too coarse to allow an explicit numerical solution. The vertical diffusive processes in the PBL and free troposphere are parameterized using local and non-local transport terms [*Boville and Bretherton*, 2003]. Both deep and shallow convection are parameterized as well [*Hack*, 1994; *Zhang and Mcfarlane*, 1995]. The treatment for convection in CAM is based on statistical models for a mesoscale ensemble of convective cloud systems that calculate mass vertical fluxes (up- and down-drafts) on the assumption that the cumulus ensemble consumes the atmospheric instability quantified by the convective available potential energy, with a characteristic timescale estimated from observations. Here, we refer to this treatment plus the host GCM as CAM.

[16] In the version of CAM developed by the Center for Multi-scale Modeling of Atmospheric Processes (CMMAP, http://www.cmmap.org), cloud processes are represented using the CRM: System for Atmospheric Modeling (SAM) [*Khairoutdinov and Randall*, 2003]. SAM is embedded in each atmospheric column of the GCM and coupled to the large-scale flow with relaxation terms [*Khairoutdinov et al.*, 2005]. Because in this study the large-scale flow is prescribed using the CTM framework, the cloud processes within the GCM cannot affect it.

[17] The cloud treatment in SPCAM is more *explicit* than that in CAM because it discretizes each GCM atmospheric column on a finer grid, and therefore it can incorporate more detailed approximations of cloud convective dynamics including the anelastic approximation and a closure scheme for small-scale turbulence. When there is local adiabatic heating, the CRM embedded in SPCAM allows convective thermals of sizes comparable to real clouds to form, and the coupling with the GCM allows the large-scale flow to affect the local flow. We use a two-dimensional version of the CRM with sixty-four 2-km-wide horizontal grid cells oriented in the East-West direction within each column of CAM, a vertical grid structure identical to that in CAM, and a time step of twenty seconds. Here, as in previous papers, we refer to this treatment as the SPCAM parameterization.

2.3. Chemical Passive Tracers

[18] To simulate the chemical passive tracers Rn and CH_3I in CAM and SPCAM, we use the Model for OZone and Related chemical Tracers (MOZART) [*Emmons et al.*, 2010; *Lemarque et al.*, 2011]. Since the sources and sinks of the tracers are calculated at the spatial and temporal resolution of the GCM, these operate in an identical manner in CAM and SPCAM.

[19] The prescribed surface emission of Rn is similar to that used in other studies [e.g., *Jacob et al.*, 1997; *Donner et al.*, 2007]. It is constant and non-zero only over non-frozen land. Its value is 10^4 atoms m^{-2} s^{-1} between 60° S and 60° and is half that between 60° N and 70° N with no emission for Greenland. Rn decays with a lifetime of 5.51 days.

[20] The prescribed surface emission of CH_3I is taken from *Bell et al.* [2002]. Monthly-mean fluxes of CH_3I are applied cyclically to all simulated years. Approximately 70% of the total emission is from the ocean and attains its peak values at mid-latitudes between spring and summer. About 24% of the total emission comes from rice paddies in south-eastern Asia with the largest occurring between June to October. Atmospheric CH_3I has a lifetime that varies between two and six days depending primarily on photolysis (99%) and secondarily on chemical reaction with the hydroxyl radical OH (1%).

2.4. Transport of the Passive Tracers

[21] There are two types of passive tracer transports in our simulations. One is the large-scale horizontal and vertical advective transport due to horizontally divergent large-scale flow that is resolved on the GCM atmospheric grid. The other is the advective and diffusive vertical transport due to PBL and cloud convective processes that is not resolved on the GCM grid balance by either large-scale convergence or divergence.

[22] Within each atmospheric column, the net vertical large-scale mass transport can be non-zero. While the net vertical convective mass transport is strictly zero, it can still cause considerable internal mixing and thereby alter the tracer concentrations in the GCM column. The operator of the large-scale transport is identical in both simulations [*Rasch et al.*, 2006] because the runs are performed in CTM mode with identical meteorology. The convective transport operating at the GCM sub-grid scale is radically different. The CAM parameterization

described in section 2.2 represents the transport of passive constituents using a formulation consistent with the magnitude of the vertical mass fluxes diagnosed by the GCM sub-grid parameterizations [*Collins et al.*, 2004]. For SPCAM, we have implemented the passive tracer transport using the advective and diffusive dynamics of the CRM [*Khairoutdinov and Randall*, 2003] by neglecting any source or sink mechanism for the tracers at the CRM scale. Given the estimates reported in section 4 of *Khairoutdinov et al.* [2008], we expect at least 70% of the vertical transport to be the result of explicitly resolved advective dynamics and the remainder of parameterized diffusive fluxes. To introduce coupling between the concentrations of the tracers simulated by the GCM and CRM, we have implemented relaxation terms for the tracer VMRs [*Khairoutdinov et al.*, 2005]. Contrary to one-way coupling applied to the meteorological fields used to drive the models in CTM mode (section 2.1), the coupling of the tracer concentration is fully bi-directional, i.e., the up-scale effects of the CRM on the tracer distributions within the parent GCM are included in our simulations.

2.5. Local Convective Index

[23] The surface emission for the tracers prescribed in our simulations is, presumably, a highly idealized approximation of the actual heterogeneous distribution of emissions (see *Bell et al.* [2002, and references therein] for CH_3I, and *Zahorowski et al.* [2004] for Rn). Therefore in addition to comparing vertical profiles of the tracer VMRs, we also compare the relative change with height in VMR. Following the formulation of a similar metric of model fidelity developed by *Bell et al.* [2002], we quantify the relative change by the Local Convective Index (LCI):

$$\mathrm{LCI} = \Delta \ln q / \Delta h, \tag{1}$$

where q is the VMR and h is the height above sea level. For short lived tracers like the ones used here, the LCI has proven to be a useful tool for analyzing the vertical convective transport biases of the models, although it cannot separate these from biases arising from large scale transport or source and sink processes. We calculate discrete approximations of equation (1) for observations and simulations using VMR values from adjacent vertical levels.

2.6. Case Studies

[24] To test the fidelity of the simulations we have used measurements from a number of field campaigns, specifically (i) PEM-Tropics A [*Hoell et al.*, 1999], (ii) PEM-Tropics B [*Raper et al.*, 2001], (iii) ACCENT [*Murphy et al.*, 1998], (iv) TRACE-P [*Jacob et al.*, 2003], (v) Pre-AVE (Pre-AURA Validation Experiment, http://www.espo.nasa.gov/missions.php), (vi) INTEX-A [*Singh et al.*, 2006], (vii) CR-AVE (Costa Rica Aura Validation Experiment, http://www.espo.nasa.gov/missions.php), (viii) INTEX-B [*Singh et al.*, 2009], (ix) ARCTAS [*Jacob et al.*, 2010], (x) ABLE-2B [*Pereira et al.*, 1991], (xi) Rn profiles from flights originating from Moffett Field, California [*Kritz et al.*, 1998], (xii) Rn profiles from a series of campaigns over mid latitude continental land in the northern hemisphere [*Liu et al.*, 1984], and (xii) PBL Rn profiles in the SE Australia [*Williams et al.*, 2011]. We have partitioned the data based on the various missions, time periods, and locations of the observations. The case studies are summarized in Table 1.

[25] *Precise* comparisons of tracer profiles are conducted using simulated VMRs for which the model time steps and grid-point coordinates are the closest to the times and locations of the observed VMRs. Specifically, for each VMR measurement, a matching VMR value is extracted from the simulation such that its discrete location is the closest to the observational location (with respect to latitude, longitude, and height) and its three-hourly time step is the closest to but less than the observational time. *Climatological* comparisons are similar but a simulated VMR value is taken from each simulated year by matching the relative time of year for each measurement. Note that for the case study ALLY07_NHCON_LIU (Table 1), the original observation time is not available for all data points, and we assume these missing times are uniformly randomly distributed between 9 a.m. and 9 p.m.. In addition, for some data points only the month in which the observations have been taken is available. For the purposes of temporal matching, we assume that dates of the measurements are uniformly distributed in that time period. Observed and simulated values are binned on discrete vertical layers of depth of 1, 3, 5, 5, and 6 Km, and midpoints at 0.5, 2.5, 6.5, 11.5, and 17 Km of altitude, respectively. We have opted for a coarse vertical grid to focus on the main feature of the profiles, and we have chosen the bins to approximately match the regions where the simulated values differ the most between models.

[26] The biases between simulations and observed LCIs are calculated on leaps between adjacent atmospheric layers which are referred to here as Planetary Boundary Layer Leap (PBLL; 0.5–2.5 Km), Low Troposphere Leap (LTL; 2.5–6.5 Km), Mid Troposphere Leap (MTL; 6.5–11.5 Km), and Upper Troposphere Leap (UTL; 11.5–17 Km).

3. Results

[27] First, we show precise and climatological comparisons between simulations and observations for the VMR vertical profiles of Rn and CH_3I. Next, we compare global and zonal climatological VMRs of the tracers.

3.1. Comparison of Modeled and Observed Methyl Iodide

[28] The root mean square errors between modeled and observationally estimated LCIs are shown in Figure 2xv after averaging over all CH_3I field campaigns listed in Table 1. Our primary general is that the mean LCI biases from SPCAM are smaller than the biases from CAM for the PBLL, MTL, and UTL, but larger for the LTL; however, the statistical uncertainty is large. LCI biases are smaller for precise comparisons than for climatological ones for the PBLL and UTL, but larger

Table 1. Case Studies Code Names for Rn and CH_3I Observations From Field Campaigns

Name	Tracer	Pts	Period	Lat × Lon [°N × °E]	Alt. [Km]	Mission	Reference	Figure
199609_ITCZ_PMT	CH_3I	533	(1996-08-21, 1996-10-05)	(0,20) × (187,227)	(0,10)	PEM-Tropics A	*Hoell et al.* [1999]	1i
199609_SPCZ_PMT	CH_3I	2242	(1996-08-31, 1996-10-05)	(-35,0) × (152,260)	(0,11)	PEM-Tropics A	*Hoell et al.* [1999]	1ii
199904_TPC_PMB	CH_3I	1612	(1999-03-06, 1999-04-13)	(-34,20) × (194,225)	(0,12)	PEM-Tropics B	*Raper et al.* [2001]	1iii
199909_UTGM_ACC	CH_3I	135	(1999-09-03, 1999-09-20)	(25,39) × (262,281)	(10,19)	ACCENT	*Murphy et al.* [1998]	1iv
200103_SCPC_TRP	CH_3I	1383	(2001-02-26, 2001-04-09)	(16,41) × (160,238)	(0,12)	TRACE-P	*Jacob et al.* [2003]	1v
200103_SWPC_TRP	CH_3I	3721	(2001-02-27, 2001-04-03)	(7,46) × (112,160)	(0,12)	TRACE-P	*Jacob et al.* [2003]	1vi
200401_UTPAN_PREAVE	CH_3I	133	(2004-01-16, 2004-02-02)	(-3,38) × (263,279)	(8,19)	Pre-AVE	N/A	1vii
200407_EUS_INTEXA	CH_3I	2654	(2004-07-06, 2004-08-14)	(27,54) × (250,324)	(0,13)	INTEX-A	*Singh et al.* [2006]	1viii
200601_UTPAN_CRAVE	CH_3I	151	(2006-01-17, 2006-02-09)	(-2,11) × (269,283)	(12,19)	CR_AVE	N/A	1ix
200603_GMEX_INTEXB	CH_3I	893	(2006-02-24, 2006-03-22)	(14,35) × (255,274)	(0,12)	INTEX-B	*Singh et al.* [2009]	2x
200604_STEPC_INTEXB	CH_3I	1058	(2006-04-17, 2006-05-15)	(19,50) × (184,235)	(0,12)	INTEX-B	*Singh et al.* [2009]	2xi
200605_GALA_INTEXB	CH_3I	369	(2006-05-01, 2006-05-15)	(50,63) × (190,225)	(0,12)	INTEX-B	*Singh et al.* [2009]	2xii
200806_SFO_ARCTAS	CH_3I	807	(2008-06-18, 2008-07-13)	(32,42) × (232,245)	(0,10)	ARCTAS	*Jacob et al.* [2010]	2xiii
200807_CAN_ARCTAS	CH_3I	699	(2008-06-26, 2008-07-13)	(45,60) × (240,278)	(0,12)	ARCTAS	*Jacob et al.* [2010]	2xiv
198705_AMAZ_A2B	Rn	54	(1987-04-20, 1987-05-08)	(-4,0) × (299,312)	(0,6)	ABLE-2B	*Pereira et al.* [1991]	3i
199407_NEPC_KRITZ	Rn	127	(1994-06-03, 1994-08-16)	(34,41) × (234,246)	(0,13)	N/A	*Kritz et al.* [1998]	3ii
ALLY07_NHCON_LIU	Rn	150	(1970-07-01, 1970-08-31)	(34,49) × (32,271)	(0,12)	N/A	*Liu et al.* [1984]	3iii
200605_ALAS	Rn	76	(2006-05-17, 2006-05-25)	(-34,-35) × (149,150)	(0,3)	N/A	*Williams et al.* [2011]	3iv
ALLY01_ALAS	Rn	71	(2007-01-19, 2007-01-25)	(-34,-35) × (149,150)	(0,3)	N/A	*Williams et al.* [2011]	3v
ALLY05_ALAS	Rn	265	(2006-05-17, 2008-05-14)	(-34,-35) × (149,150)	(0,3)	N/A	*Williams et al.* [2011]	3vi

for the LTL and MTL. The mean differences between the modeled and observed VMR profiles and the resulting LCI values constructed by averaging over each individual field campaign are displayed in Figures 1 and 2. In general, both models overestimate the decrease of CH_3I VMR with altitude in every layer except for the MTL. The VMR from SPCAM and CAM profiles differ from each other from a few to tens of percent. The biases in SPCAM and CAM, which can be about one or two orders of magnitude at altitudes below 10 Km and at 18 Km, respectively, (Figures 1iv and 1ix), are generally greater than the differences between the two models.

[29] We provide more details about the comparisons in the following paragraphs and comment on some of them to highlight some peculiarities of individual or several case studies.

[30] Over the central tropical Pacific ocean and the South Pacific Convergence Zone, the models have negative CH_3I VMR biases in the mid and upper troposphere (Figures 1i, 1ii, and 1iii). The simulated profile is close to the observed one up to approximately 2.5 Km, above which it decreases quickly. The biggest LCI biases occur for the LTL, whereas the smallest ones occur in the PBLL. The LCI biases in SPCAM are smaller than those in CAM for the PBLL but bigger for the LTL.

[31] Over the sub-tropical Pacific ocean, the models have positive CH_3I VMR biases in the low troposphere with smaller biases in the mid and upper troposphere (Figures 1v, 1vi, and 2xi). Contrary to the case studies over the central tropical Pacific ocean and the South Pacific Convergence Zone, the biggest LCI biases occur for the PBLL whereas the smallest ones occur for the LTL. LCI biases in SPCAM are smaller than those in CAM for the PBLL but bigger for the LTL.

[32] Over the east coast of the United States, the models have no CH_3I VMR biases in the PBL, but they have negative biases in the mid and upper troposphere (Figure 1viii). The LCI biases in both models are notably large and negative for the PBLL; LTL LCI biases are negative for SPCAM and positive for CAM, whereas MTL LCI biases are positive for both models. A possible interpretation of these features is that CAM, and to a lesser degree SPCAM, may have not enough mixing in the PBL or may be depleting the cloud layer too much between 1 and 4 Km due to excessive convective activity. Precise and climatological comparisons have comparable LCI biases.

[33] Over the Gulf of Mexico, the models have negative CH_3I VMR biases increasing with altitude (Figure 2x). The LCI biases in SPCAM are smaller than those in CAM for the PBLL and MTL, and bigger for the LTL. Climatological comparisons have smaller LCI biases than precise comparisons, especially for the MTL.

[34] Over the Gulf of Alaska, the models have positive CH_3I VMR biases in the PBL that decrease with altitude (Figure 2xii). The LCI biases in SPCAM are smaller than those in CAM for the PBLL, but comparable for the LTL and MTL. In the PBL, the LCI biases from the precise comparison are much smaller than the corresponding climatological biases. This case study shows that both models can respond properly to large-scale

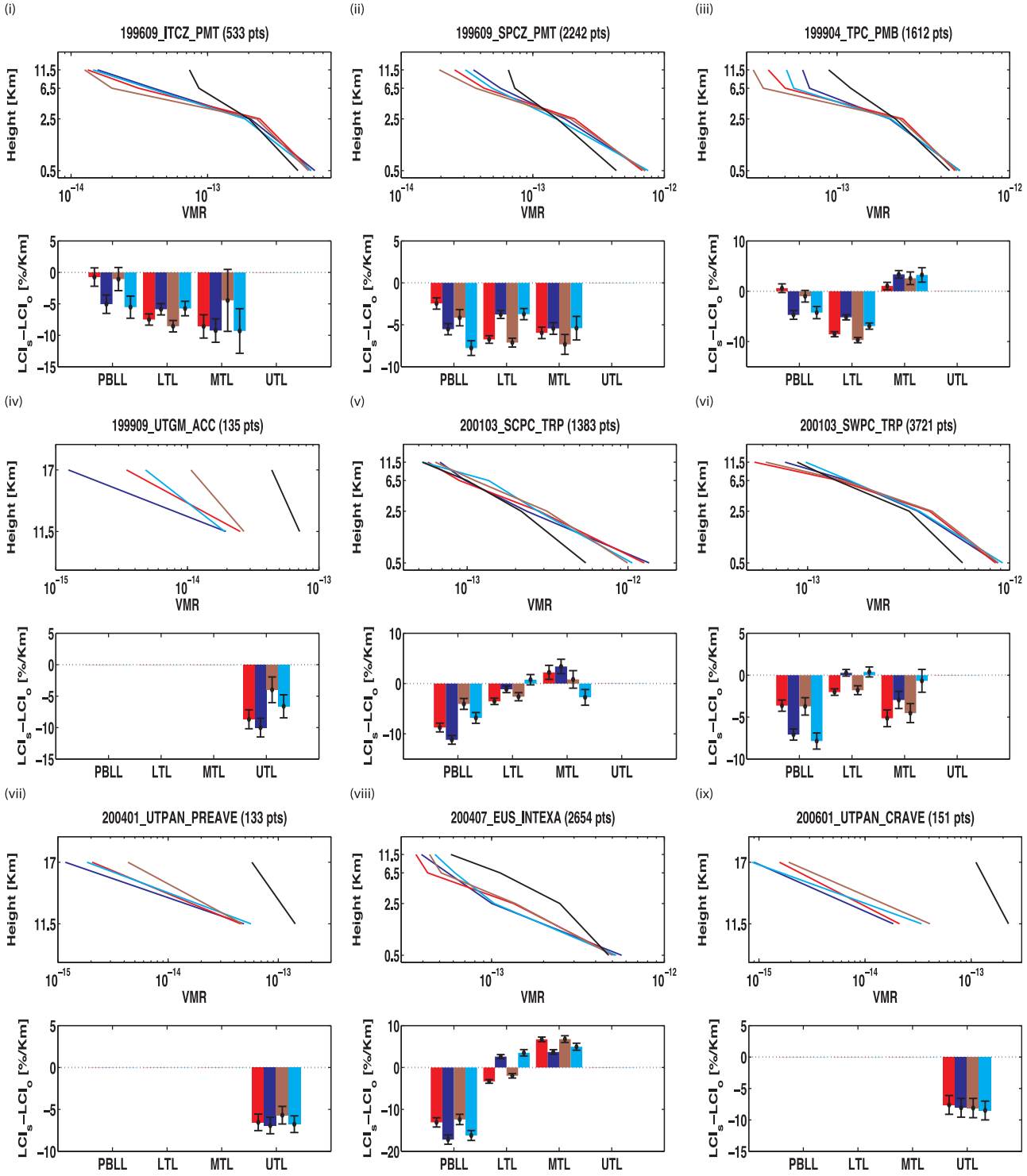

Figure 1. See caption of Figure 2.

conditions and reproduce better estimates of real tracer distributions. We do not find a similar difference between precise and climatological comparisons for the other case studies possibly due to the little sensitivity of the models to or errors in the other large-scale conditions.

[35] Over the San Francisco Bay and Canada, the models look similar. They have positive CH_3I VMR biases in the PBL and negative biases in the upper troposphere (Figure 2xiii and 2xiv). These are regions of low average rainfall and convective activity. Nonetheless, the LCI biases from SPCAM are smaller than those over CAM for the PBLL over CANADA (Figure 2xiv). SPCAM does not deplete the layer between 1 and 4 Km as much as CAM does, resulting in a better match with the VMR change with height of

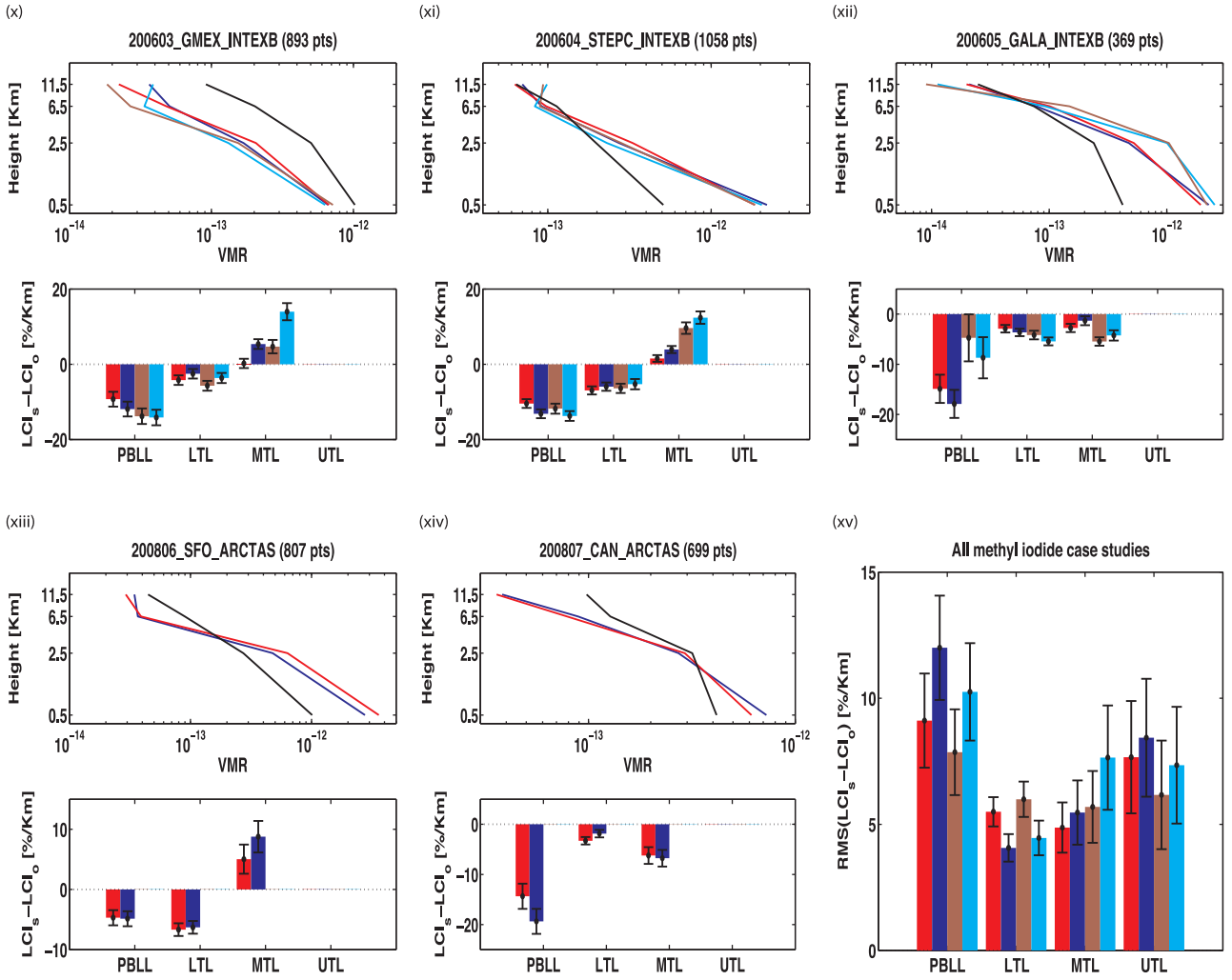

Figure 2. Comparisons between simulated and observed vertical profiles and LCI biases in the PBLL, LTL, MTL, and UTL for CH_3I. Climatological/precise values are shown in red/brown for SPCAM and blue/cyan for CAM, respectively. Observed profiles are shown in black. Standard errors are not shown because they are much smaller than the differences between mean values. Below each profile comparison, LCI biases are shown with bars at one standard error. Figure 2xi shows the root mean square (RMS) and its standard error for LCI biases in all the profiles.

the observed tracer. This again suggests an underestimation of mixing in the PBL by CAM and, to a lesser degree, SPCAM.

[36] For the profiles at high altitude between 9 to 20 Km, over the Central Americas, the models consistently underestimate the observed CH_3I VMR (Figures 1iv, 1vii, and 1ix). However, the VMR and LCI biases from SPCAM are smaller than those from CAM. We suspect this could be due to convective overshooting at the CRM scale, a feature that is missing in CAM. Precise comparisons have smaller LCI biases than climatological ones only for one case study (Figure 1iv).

3.2. Comparison of Modeled and Observed Radon

[37] Mean VMR profiles and LCI biases for simulated Rn are shown in Figure 3. For the coastal mid latitude case (Figure 3ii), climatological VMRs from SPCAM and CAM look similar. This is also the result for a CH_3I case referring to a nearby location (Figure 2xiii). We interpret the similarity of the models to lack of vertical transport by convective processes that are the primary source of the differences between simulated profiles. Rn has a longer lifetime than CH_3I, and the factors that determine LCI of the models in the MTL are the contribution of Rn emitted upwind of the case study site in Asia and the integrated vertical and horizontal transport (results not shown; we used different tags for Rn emitted in the Americas and Eurasia). We show that the MTL LCI bias from SPCAM is slightly smaller although this result has little statistical confidence. Another continental case is a reconstruction using more heterogeneous measurements in time and space that has often been used in studies similar to ours (Figure 3iii) [*Liu et al.*, 1984]. We assert that the similarity between

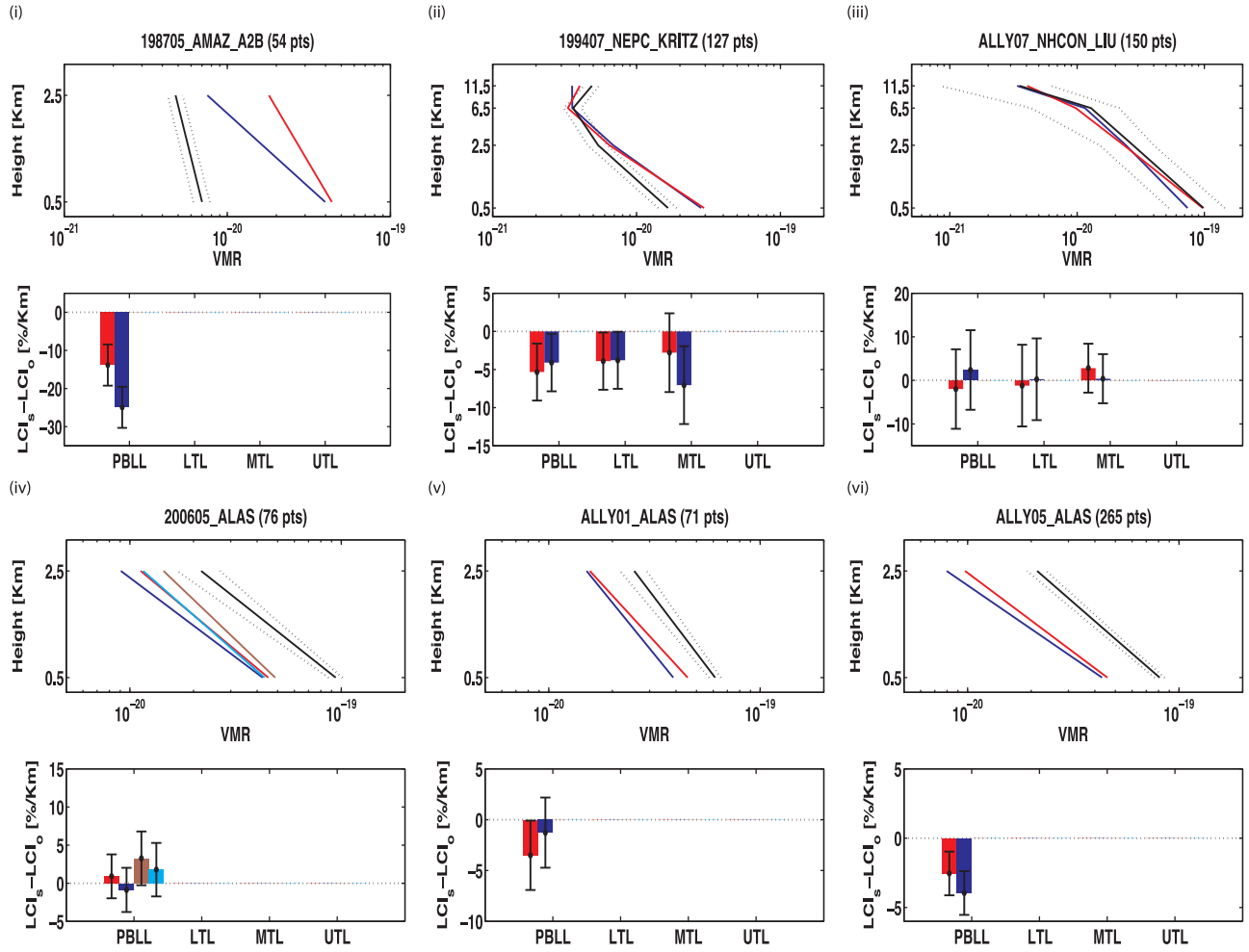

Figure 3. Comparisons between simulated and observed vertical profiles and LCI biases in the PBLL, LTL, and MTL for Rn. Climatological/precise values are shown in solid red/brown for SPCAM and solid blue/cyan for CAM, respectively. Observed profiles are shown in black. Standard errors are shown in dashed black and only for observed values because the standard errors for the models are much smaller than the differences between mean values. Below each profile comparison, LCI biases relative to the observations are shown with error bars in black at one standard error.

models is the result of averaging across heterogeneous sampling locations. The LCI biases from SPCAM are bigger than those from CAM and the statistical confidence is even smaller than the prior case.

[38] The remaining case studies are limited to the first 4 Km in height and refer to two climatologically very different regions. Over the wet tropical Amazon forest, models have positive Rn VMR biases (Figure 3i; for this case study, *Pereira et al.* [1991] estimated a ground flux between 1/2 and 1/3 of what we prescribed here). The LCI biases from SPCAM LCI biases are much smaller than those from CAM for the PBLL, confirming the general conclusions for the CH_3I case studies. Over the SE Australia, a region with little mean rainfall, models have negative Rn VMR biases (Figures 3iv, 3v, and 3vi). The SPCAM LCI biases are bigger than those of CAM in two cases (Figures 3iv and 3v). For one case, precise comparisons have bigger biases than climatological ones (Figure 3iv). For the case study with the biggest measurement sample size, the PBLL LCI bias in SPCAM is smaller than that in CAM.

3.3. Global Patterns From Simulations

[39] Some coherent patterns associated with the regions of cloud convective activity are evident in the differences between zonal and global time-mean distributions of Rn and CH_3I by CAM and SPCAM. We focus on the broad features for the low and mid latitudes and, implying all altitudes in an approximate sense, consider 4 vertical areas: the PBL between the surface and 1 Km, the LT between 1 and 4 Km, the MT to UT region between 4 and 12 Km, and the UT to LS region above 12 Km. In general, at latitudes where most of the convective activity occurs in the tropics and subtropics, SPCAM introduces a vertical quadrupole pattern of VMR differences relative to CAM. The quadrupole is characterized by depletion of the PBL, enrichment of the LT, depletion of the MT to UT, and enhancement of the

UT to lower stratosphere (LS) (Figure 4). We provide interpretations of the simulated patters using model outputs averaged at the GCM grid level to relate the patterns to the underlying physical processes. The convective mass fluxes look reasonable for both models, but we do not show these fields because the fluxes have different definitions and hence are not directly comparable. For SPCAM, the fluxes are defined at the CRM grid-scale and involve threshold parameters for the vertical velocity and water path, whereas for CAM the fluxes are calculated by the deep and shallow convective parameterizations at the GCM grid-scale.

[40] For the transport of short-lived tracers like the ones implemented here, *Lawrence and Rasch* [2005] have studied the implications of decomposing the deep convective scheme in CAM from its "bulk" implementation into its original "plume" formulation. They find a pattern for the fractional differences in the simulated VMRs that is similar to our results for the MT to UT and UT to LS (Figure 4ii, and Figure 4 of *Lawrence and Rasch* [2005]). SPCAM is an explicit plume scheme, and we believe that the same arguments they used to described their results are valid for ours. Their hypothesis is that minimally-entraining plumes can carry higher tracer amounts to high altitudes. However, there are some appreciable differences. Our results show a stronger pattern and apply to Rn which, with its lifetime of about 5 days, should reveal a moderate difference between the models. Moreover, we find that the PBL is depleted and the LT is enriched for SPCAM (Figure 4ii). In a numerical experiment of tracer transport by mesoscale convective systems where a 2D CRM is forced with large-scale conditions derived from the observations, *Lu et al.* [2000] have shown that simulated deep convection can transport PBL air to the upper troposphere and overshoot through the tropopause on short timescales and with minimal dilutions. These processes could be present in our experiment and could be contributing to the difference in the UT to LS and, in addition, could explain the differences in the PBL tracer VMRs between SPCAM and CAM. In other words, by vertically advecting near-surface air, rich in tracer amount, directly to the UT, SPCAM could be making the PBL more depleted with respect to CAM, which convective mass flux starts higher, at the cloud-base. The last consideration could provide a possible explanation for the enriched LT for SPCAM. Because CAM's convective mass fluxes originate at the cloud base, which falls on average in the LT, it could more efficiently deplete the concentration at that level.

[41] In Figure 5, we show global distributions of the tracer VMRs and relative VMR differences between

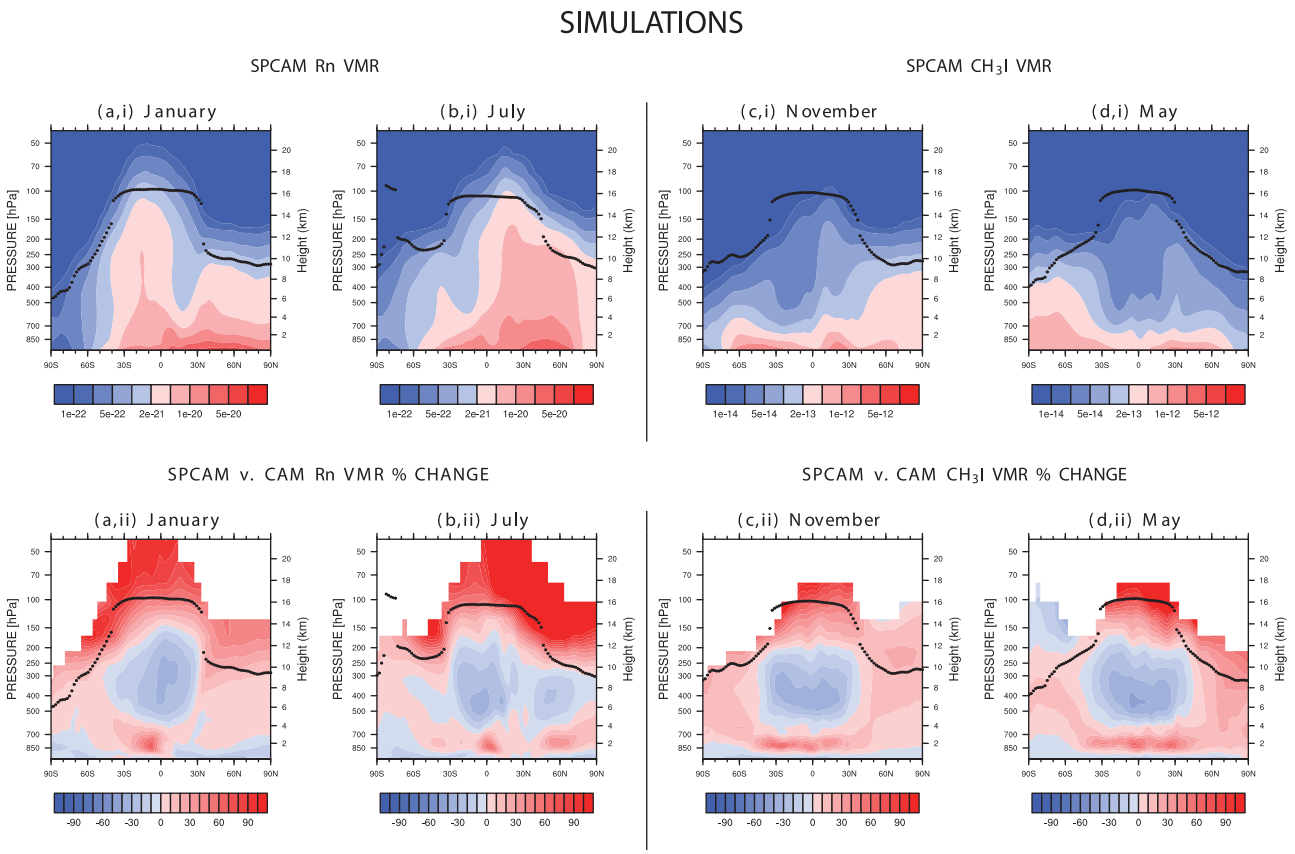

Figure 4. Simulated zonal climatologies for Rn for (a) January and (b) July, and for CH_3I for (c) November, and (d) May. (i) The total VMR is plotted on a logarithmic color scheme and (ii) SPCAM versus CAM percentage differences. We blank out the areas in which the VMR is three orders of magnitude below the global average between ground and 500 mb. The tropopause line is marked in black.

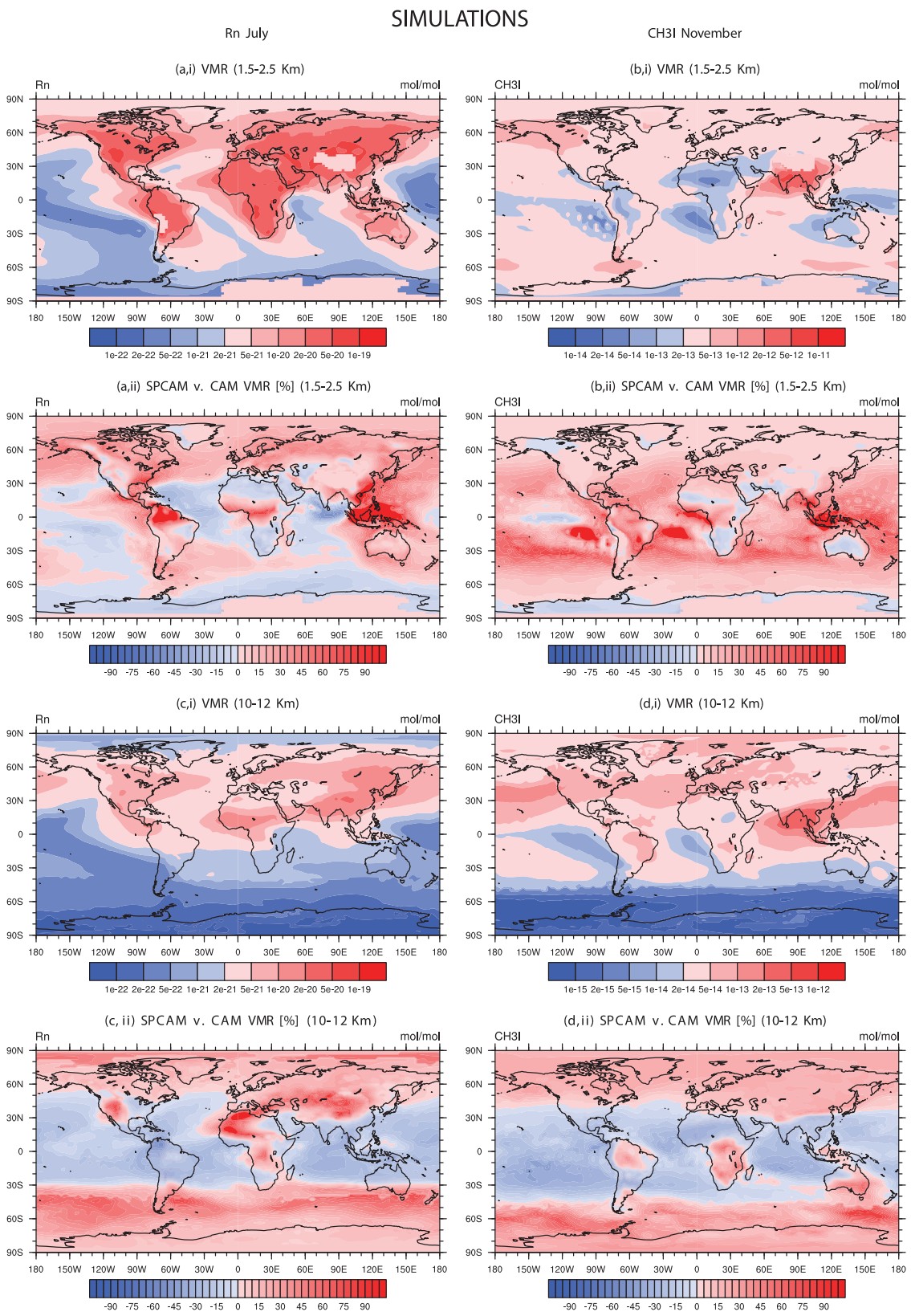

Figure 5. Simulated global climatologies (a, b) for Rn for July and (c, d) for CH_3I for November, vertically averaged from 1.5 to 2.5 (Figures 5a and 5b) and from 10 to 12 Km of altitude (Figures 5c and 5d). (i) The total VMR is plotted on a logarithmic color scheme and (ii) SPCAM versus CAM percentage differences.

SPCAM and CAM for an atmospheric layer in the LT between 1.5 and 2.5 Km and one in the UT between 10 and 12 Km.

[42] In general, SPCAM is depleted over dry regions and enriched over wet ones relative to CAM in the LT. For example, SPCAM is depleted in Rn over dry areas such as south-western U.S.A., northern Africa, and south-western Asia during July (Figure 5aii). SPCAM is enriched over very wet areas in the tropical and subtropical bands such as south-eastern U.S.A., central and northern south America, central Africa, and Indonesia, during July and November (Figure 5aii). In the UT over the dry regions, SPCAM is enriched (Figures 5c and 5dii). Also, over some wet regions, such as central Africa, the Amazon Forest, and portion of Indonesia, SPCAM is relatively enriched (Figures 5c and 5dii). Everywhere else, SPCAM is depleted and enriched relative to CAM just below and above the tropopause, respectively (Figures 4b and 4cii). We hypothesize that SPCAM is enriched in the LT because it could have stronger mixing in the PBL and because its convective mass fluxes are not concentrated at the cloud base in distinction to CAM. We also infer that SPCAM is depleted in the MT to UT because nearly non-entraining convective plumes could reach higher altitudes without mixing. For the dry regions, the GCM sub-grid vertical transport in CAM is due to the non-local PBL scheme and the shallow convection parameterization that can provide some non-local transport between non-adjacent vertical levels. However, in principle, the CRM in SPCAM could develop a more efficient vertical transport by generating dry thermals able to transport near-surface air directly to higher altitudes.

4. Summary

[43] We have tested the effects of an explicit treatment for atmospheric convective processes on the fidelity of global simulations of two short-lived passive chemical tracers by comparing simulated profiles against an extensive array of aircraft observations. Contrary to the conventional highly parametric treatment in CAM and all other conventional GCMs, SPCAM introduces a CRM within each GCM grid box to simulate the physical and dynamical atmospheric processes at scales comparable to those of individual cloud systems. We operate CAM and SPCAM in chemical transport mode in order to isolate and differentiate the effects due only to the parameterized and explicit treatments of sub-grid vertical convective motion.

[44] Comparing modeled results with observations for CH_3I, we find that the maximum differences between CAM and SPCAM are generally much smaller than the maximum biases between models and observations. The differences between models typically range from a few percent to tens of percent, while the differences between models and aircraft data range from one to two orders of magnitude. We have quantified modeled biases in simulating the relative changes of the observed tracer VMRs with height (the Local Convective Index, or LCI) for several atmospheric layers.

[45] In general, despite the large statistical uncertainties, SPCAM generates smaller LCI biases for the PBLL, MTL, and UTL, but larger for the LTL. With respect to observations, both models simulate larger vertical gradients in concentrations of CH_3I. These enhanced gradients could arise from a weaker vertical transport, stronger horizontal tracer divergence, stronger photochemical sinks, or a combination of all of these mechanisms, but further analysis is necessary to isolate the causes.

[46] For the majority of the CH_3I case studies, it is possible to contrast climatological and precise comparisons. The first is obtained using multiple simulated years and the latter is obtained using the meteorological reanalysis of the period matching the time the observations were collected. In general, for both models, precise comparisons do not appear to be definitively better or worse than climatological comparisons. This could be because the vertical transport by convective processes is not very sensitive to the meteorological variability or because of biases in the meteorological reanalysis product we used.

[47] Contrasting only results from simulations, we find a quadrupole pattern for the differences between SPCAM and CAM. In the tropics and subtropics where most of the convective precipitation occurs, SPCAM depletes the PBL, enriches the LT, depletes the MT up to approximately 2 Km below the tropopause, and enriches the UT and above relative to CAM. The CRMs embedded in SPCAM allow air parcels to be advected vertically from the surface to any altitude in the model grids. This could result in a greater net vertical transport of tracer-enriched air from less diluted air parcels with respect to a treatment that does not explicitly resolve the physics of convection.

[48] From contrasting models with observations, we have found some indications that SPCAM can simulate the transport of short-lived surface-emitted passive tracers more realistically than CAM. Comparing the simulated tracer distributions of CAM and SPCAM could help design field campaigns for areas where the differences between the models are the greatest. This would help diagnose which model is generally closer to reality.

[49] Our results, although preliminary and requiring further validation, invite speculation about their implications for atmospheric chemistry and climate. The explicit and the conventional treatment of cloud processes from SPCAM and CAM produce considerable percentage differences in the short-lived compounds evaluated in this study. Our results suggest that SPCAM vertical transport could produce different estimates of the radiative forcing from ozone and its precursors, or from reflecting aerosols as a function of their vertical location with respect to clouds. It could also imply novel dynamical interactions between clouds and their dissipating or promoting compounds. With respect to air quality, the explicit cloud treatment result in a PBL with lower concentrations of compounds emitted by the surface and more efficient high-level long-range transport of these compounds by mid-latitude jets.

These implications will be examined in future studies with the Multi-scale Modeling Framework.

[50] **Acknowledgments.** This work was supported by Contractor Supporting Research (CSR) funding from Berkeley Lab, provided by the Director, Office of Science, of the U.S. Department of Energy under contract DE-AC02-05CH11231. This material is also supported by the National Science Foundation Science and Technology Center for Multi-scale Modeling of Atmospheric Processes CMMAP, managed by Colorado State University under cooperative agreement ATM-0425247. National Center for Atmospheric Research (NCAR) is sponsored by the NSF. We thank the National Center for Atmospheric Research, operated by the University Corporation for Atmospheric Research under sponsorship of the National Science Foundation. We specifically acknowledge the assistance of Francis Vitt and Simone Tilmes. We would like to acknowledge high-performance computing support provided the Computational and Information Systems Laboratory at NCAR, also sponsored by the National Science Foundation. We acknowledge high-performance computing and support provided by Xsede. We acknowledge the LaRC Airborne Science Data for Atmospheric Composition and The Earth Science Project Office (ESPO) Data Archive at NASA for collecting and making the field campaigns data available. We thank Leo Donner (GFDL/NOAA, USA), Chris Bretherton (UW, USA), and Marat Khairoutdinov (SOMAS, USA) for their useful comments and the discussions we had. We thank Alastair G. Williams (ANSTO, Australia) for helping incorporating his recent radon data in our study. We thank the anonymous reviewers for helping us improving the paper.

References

Bell, N., L. Hsu, D. J. Jacob, M. G. Schultz, D. R. Blake, J. H. Butler, D. B. King, J. M. Lobert, and E. Maier-Reimer (2002), Methyl iodide: Atmospheric budget and use as a tracer of marine convection in global models, *J. Geophys. Res.*, *107*(D17), 4340, doi:10.1029/2001JD001151.

Boville, B., and C. Bretherton (2003), Heating and kinetic energy dissipation in the NCAR Community Atmosphere Model, *J. Clim.*, *16*(23), 3877–3887, doi:10.1175/1520-0442(2003)016<3877:HAKEDI>2.0.CO;2.

Collins, W., et al. (2004), Description of the NCAR Community Atmosphere Model (CAM 3.0), *NCAR Tech. Note NCAR-464+STR*, Natl. Cent. for Atmos. Res., Boulder, Colo.

Collins, W., et al. (2006), The formulation and atmospheric simulation of the Community Atmosphere Model version 3 (CAM3), *Journal Of Climate*, *19*(11), 2144–2161, doi:10.1175/JCLI3760.1.

Donner, L. J., L. W. Horowitz, A. M. Fiore, C. J. Seman, D. R. Blake, and N. J. Blake (2007), Transport of radon-222 and methyl iodide by deep convection in the GFDL Global Atmospheric Model AM2, *J. Geophys. Res.*, *112*, D17303, doi:10.1029/2006JD007548.

Emmons, L. K., et al. (2010), Description and evaluation of the Model for Ozone and Related chemical Tracers, version 4 (MOZART-4), *Geosci. Model Dev.*, *3*(1), 43–67, doi:10.5194/gmd-3-43-2010.

Folkins, I., P. Bernath, C. Boone, L. J. Donner, A. Eldering, G. Lesins, R. V. Martin, B.-M. Sinnhuber, and K. Walker (2006), Testing convective parameterizations with tropical measurements of HNO_3, CO, H_2O, and O_3: Implications for the water vapor budget, *J. Geophys. Res.*, *111*, D23304, doi:10.1029/2006JD007325.

Forster, P., et al. (2007), Changes in atmospheric constituents and radiative forcing, in *Climate Change 2007: The Physical Science Basis. Contribution of Workng Group I to the Fourth Assessment Report of the Intergovernmental Panel on Climate Change*, edited by S. Solomon et al., pp. 129–234, Cambridge Univ. Press, Cambridge, U. K.

Hack, J. J. (1994), Parameterization of moist convection in the National Center for Atmospheric Research community climate model (CCM2), *J. Geophys. Res.*, *99*(D3), 5551–5568, doi:10.1029/93JD03478.

Hoell, J. M., D. D. Davis, D. J. Jacob, M. O. Rodgers, R. E. Newell, H. E. Fuelberg, R. J. McNeal, J. L. Raper, and R. J. Bendura (1999), Pacific Exploratory Mission in the tropical Pacific: PEM-Tropics A, August–September 1996, *J. Geophys. Res.*, *104*(D5), 5567–5583, doi:10.1029/1998JD100074.

Hoyle, C. R., et al. (2011), Representation of tropical deep convection in atmospheric models—Part 2: Tracer transport, *Atmos. Chem. Phys.*, *11*(15), 8103–8131, doi:10.5194/acp-11-8103-2011.

Jacob, D. J., et al. (1997), Evaluation and intercomparison of global atmospheric transport models using ^{222}Rn and other short-lived tracers, *J. Geophys. Res.*, *102*(D5), 5953–5970, doi:10.1029/96JD02955.

Jacob, D. J., J. H. Crawford, M. M. Kleb, V. S. Connors, R. J. Bendura, J. L. Raper, G. W. Sachse, J. C. Gille, L. Emmons, and C. L. Heald (2003), Transport and Chemical Evolution over the Pacific (TRACE-P) aircraft mission: Design, execution, and first results, *J. Geophys. Res.*, *108*(D20), 9000, doi:10.1029/2002JD003276.

Jacob, D. J., et al. (2010), The Arctic research of the composition of the troposphere from aircraft and satellites (arctas) mission: Design, execution, and first results, *Atmos. Chem. Phys.*, *10*(11), 5191–5212, doi:10.5194/acp-10-5191-2010.

Kalnay, E., et al. (1996), The NCEP/NCAR 40-year reanalysis project, *Bull. Am. Meteorol. Soc.*, *77*(3), 437–471, doi:10.1175/1520-0477(1996)077<0437:TNYRP>2.0.CO;2.

Khairoutdinov, M., and D. Randall (2003), Cloud resolving modeling of the ARM summer 1997 IOP: Model formulation, results, uncertainties, and sensitivities, *J. Atmos. Sci.*, *60*(4), 607–625, doi:10.1175/1520-0469(2003)060<0607:CRMOTA>2.0.CO;2.

Khairoutdinov, M., D. Randall, and C. Demott (2005), Simulations of the atmospheric general circulation using a cloud-resolving model as a superparameterization of physical processes, *J. Atmos. Sci.*, *62*(7), 2136–2154, doi:10.1175/JAS3453.1.

Khairoutdinov, M., C. DeMott, and D. Randall (2008), Evaluation of the simulated interannual and subseasonal variability in an AMIP-Style simulation using the CSU multiscale modeling framework, *J. Clim.*, *21*(3), 413–431, doi:10.1175/2007JCLI1630.1.

Kritz, M. A., S. W. Rosner, and D. Z. Stockwell (1998), Validation of an off-line three-dimensional chemical transport model using observed radon profiles: 1. Observations, *J. Geophys. Res.*, *103*(D7), 8425–8432, doi:10.1029/97JD02655.

Lamarque, J.-F., et al. (2011), CAM-chem: Description and evaluation of interactive atmospheric chemistry in CESM, *Geosci. Model Dev. Discuss.*, *4*(3), 2199–2278, doi:10.5194/gmdd-4-2199-2011.

Lawrence, M., and P. Rasch (2005), Tracer transport in deep convective updrafts: Plume ensemble versus bulk formulations, *J. Atmos. Sci.*, *62*(8), 2880–2894, doi:10.1175/JAS3505.1.

Lelieveld, J., and P. J. Crutzen (1994), Role of deep cloud convection in the ozone budget of the troposphere, *Science*, *264*(5166), 1759–1761, doi:10.1126/science.264.5166.1759.

Lemone, M. A., and E. J. Zipser (1980), Cumulonimbus vertical velocity events in Gate. 1. Diameter, intensity and mass flux, *J. Atmos. Sci.*, *37*(11), 2444–2457, doi:10.1175/1520-0469(1980)037<2444:CVVEIG>2.0.CO;2.

Liu, S. C., J. R. McAfee, and R. J. Cicerone (1984), Radon 222 and tropospheric vertical transport, *J. Geophys. Res.*, *89*(D5), 7291–7297, doi:10.1029/JD089iD05p07291.

Lu, R., C. Lin, R. Turco, and A. Arakawa (2000), Cumulus transport of chemical tracers: 1. Cloud-resolving model simulations, *J. Geophys. Res.*, *105*(D8), 10,001–10,021, doi:10.1029/2000JD900009.

Lucas, C., E. J. Zipser, and M. A. Lemone (1994), Vertical velocity in oceanic convection off tropical australia, *J. Atmos. Sci.*, *51*(21), 3183–3193, doi:10.1175/1520-0469(1994)051<3183:VVIOCO>2.0.CO;2.

Mahowald, N. M., P. J. Rasch, and R. G. Prinn (1995), Cumulus parameterizations in chemical transport models, *J. Geophys. Res.*, *100*(D12), 26,173–26,189, doi:10.1029/95JD02606.

Mahowald, N. M., P. J. Rasch, B. E. Eaton, S. Whittlestone, and R. G. Prinn (1997), Transport of ^{222}*J. Geophys. Res.*, *102*(D23), 28,139–28,151.

May, P., and D. Rajopadhyaya (1999), Vertical velocity characteristics of deep convection over Darwin, Australia, *Mon. Weather Rev.*, *127*(6), 1056–1071, doi:10.1175/1520-0493(1999)127<1056:VVCODC>2.0.CO;2.

Murphy, D., D. Thomson, and T. Mahoney (1998), In situ measurements of organics, meteoritic material, mercury, and other elements in aerosols at 5 to 19 kilometers, *Science*, *282*(5394), 1664–1669, doi:10.1126/science.282.5394.1664.

Pereira, E. B., P. L. Silva Dias, and D. J. Nordemann (1991), Radon concentrations profiles over the Brazilian Amazon basin during the wet season, *Rev. Bras. Geofis.*, *91*(2), 61–68.

Ramaswamy, V., et al. (2001), Radiative forcing of climate change, in *Climate Change 2001: The Scientific Basis. Contribution of Working Group I to the Third Assessment Report of the Intergovernmental Panel on Climate Change*, edited by D. J. Griggs et al., pp. 405–416, Cambridge Univ. Press, Cambridge, U. K.

Raper, J. L., M. M. Kleb, D. J. Jacob, D. D. Davis, R. E. Newell, H. E. Fuelberg, R. J. Bendura, J. M. Hoell, and R. J. McNeal (2001), Pacific Exploratory Mission in the tropical Pacific: PEM-Tropics B,

March–April 1999, *J. Geophys. Res.*, *106*(D23), 32,401–32,425, doi:10.1029/2000JD900833.

Rasch, P. J., D. B. Coleman, N. Mahowald, D. L. Williamson, S.-J. Lin, B. A. Boville, and P. Hess (2006), Characteristics of atmospheric transport using three numerical formulations for atmospheric dynamics in a single GCM framework, *J. Clim.*, *19*(11), 2243–2266, doi:10.1175/JCLI3763.1.

Schulz, M., et al. (2006), Radiative forcing by aerosols as derived from the aerocom present-day and pre-industrial simulations, *Atmos. Chem. Phys.*, *6*, 5225–5246, doi:10.5194/acp-6-5225-2006.

Singh, H. B., W. H. Brune, J. H. Crawford, D. J. Jacob, and P. B. Russell (2006), Overview of the summer 2004 Intercontinental Chemical Transport Experiment–North America (INTEX-A), *J. Geophys. Res.*, *111*, D24S01, doi:10.1029/2006JD007905.

Singh, H. B., W. H. Brune, J. H. Crawford, F. Flocke, and D. J. Jacob (2009), Chemistry and transport of pollution over the Gulf of Mexico and the Pacific: Spring 2006 INTEX-B campaign overview and first results, *Atmos. Chem. Phys.*, *9*(7), 2301–2318, doi:10.5194/acp-9-2301-2009.

Stevenson, D. S., et al. (2006), Multimodel ensemble simulations of present-day and near-future tropospheric ozone, *J. Geophys. Res.*, *111*, D08301, doi:10.1029/2005JD006338.

Tang, Q., M. J. Prather, and J. Hsu (2011), Stratosphere-troposphere exchange ozone flux related to deep convection, *Geophys. Res. Lett.*, *38*, L03806, doi:10.1029/2010GL046039.

Tost, H., M. G. Lawrence, C. Bruehl, P. Joeckel, GABRIEL Team, and SCOUT-O3-DARWIN ACTIVE Team (2010), Uncertainties in atmospheric chemistry modelling due to convection parameterisations and subsequent scavenging, *Atmos. Chem. Phys.*, *10*(4), 1931–1951, doi:10.5194/acp-10-1931-2010.

Uma, K. N., and T. N. Rao (2009), Characteristics of vertical velocity cores in different convective systems observed over Gadanki, India, *Mon. Weather Rev.*, *137*(3), 954–975, doi:10.1175/2008MWR2677.1.

Williams, A. G., W. Zahorowski, S. Chambers, A. Griffiths, J. M. Hacker, A. Element, and S. Werczynski (2011), The vertical distribution of radon in clear and cloudy daytime terrestrial boundary layers, *J. Atmos. Sci.*, *68*(1), 155–174, doi:10.1175/2010JAS3576.1.

World Health Organization (2006), *Air Quality Guidelines Global Update 2005: Particulate Matter, Ozone, Nitrogen Dioxide and Sulfur Dioxide*, WHO Reg. Off. for Eur., Copenhagen.

Xie, S., et al. (2002), Intercomparison and evaluation of cumulus parametrizations under summertime midlatitude continental conditions, *Q. J. R. Meteorol. Soc.*, *128*(582), 1095–1135, doi:10.1256/003590002320373229.

Xu, K., et al. (2002), An intercomparison of cloud-resolving models with the atmospheric radiation measurement summer 1997 intensive observation period data, *Q. J. R. Meteorol. Soc.*, *128*(580), 593–624, doi:10.1256/003590002321042117.

Zahorowski, W., S. Chambers, and A. Henderson-Sellers (2004), Ground based radon-222 observations and their application to atmospheric studies, *J. Environ. Radioact.*, *76*(1–2), 3–33, doi:10.1016/j.jenvrad.2004.03.033.

Zhang, G., and N. Mcfarlane (1995), Sensitivity of climate simulations to the parameterization of cumulus convection in the Canadian Climate Center general-circulation model, *Atmos. Ocean*, *33*(3), 407–446, doi:10.1080/07055900.1995.9649539.

Zhang, K., H. Wan, M. Zhang, and B. Wang (2008), Evaluation of the atmospheric transport in a GCM using radon measurements: Sensitivity to cumulus convection parameterization, *Atmos. Chem. Phys.*, *8*(10), 2811–2832, doi:10.5194/acp-8-2811-2008.

Corresponding author: D. Rosa, Department of Earth and Planetary Science, University of California, 413 McCone Hall #4767, Berkeley, CA 94720-4767, USA. (drosa@berkeley.edu)